Assiut University Journal of Multidisciplinary Scientific Research (AUNJMSR)
Faculty of Science, Assiut University, Assiut, Egypt.
Printed ISSN 2812-5029
Online ISSN 2812-5037
Vol. 53(3): 385- 412 (2024)
https://aunj.journals.ekb.eg

Casson Nanofluid Flow Through Tissue Incorporating an Inclined Cylindrical Lymphatic Vessel

N. F. Ahmed [1,*], M. A. Mansour [1] , F. S. Ibrahim [1] and A. M. Ismaeel [2]
[1]Department of Mathematics, Faculty of Science, Assiut University, Assiut, Egypt.
[2]Faculty of Basic Sciences, King Salman International University, Ras Sudr, South Sinai, Egypt.

[*]Corresponding Author: nora.20121211@science.aun.edu.eg

ARTICLE INFO

Article History:
Received: 2024-05-29
Accepted: 2024-07-18
Online: 2024-08-29

Keywords:
Lymphatic vessels; Drug delivery; mass and heat transport; Casson nanofluid; mixed convection; similarity transformations.

ABSTRACT

This theoretical study aims to explore the dynamics of a Casson nanofluid flowing through a biological tissue under the influence of a magnetic field, in the presence of an inclined circular cylindrical lymphatic vessel. The governing partial differential equations and their boundary conditions are transformed into a set of non-linear ordinary differential equations using appropriate similarity transformations. The problem is solved using the bvp4c function in MATLAB software, and the numerical results are presented graphically. The research investigates and visually depicts the impact of various parameters on the velocity of the nanofluid, its temperature, and the concentration of nanoparticles. These parameters encompass the magnetic field, porous medium, inclination angle, thermophoresis, thermal Grashof number, Eckert number, mass Grashof number, Casson parameter, and the curvature parameter. The study concludes that an increase in the value of the Casson parameter significantly elevates the NP concentration while concurrently reducing the temperature of the nanofluid. We also found that there is a decreasing trend in both the nanofluid temperature and the NP concentration. The two variables peak in the tissue and then drop close to the lymph channel wall.

1. INTRODUCTION

The field of nanofluids has recently garnered significant attention due to their unique rheological and thermal properties [1]. These properties have been extensively studied both numerically and experimentally by researchers worldwide, aiming to gain a deeper understanding and evaluate their potential in various applications. Among these applications, the behavior of nanofluids in porous media is of particular interest, especially in the realm of biomedical engineering [2].

The term "nanofluid" was first coined by Choi and Eastman [3], who discovered that the enhanced thermal conductivity of the base fluid could be attributed to the nanoscale particles suspended within it. Boungiorno [4] further investigated the factors contributing to the improved heat transfer in nanofluids and proposed that thermophoresis and Brownian diffusion played a significant role. Building on Buongiorno's model, Hashim et al. [5] developed a mathematical framework to simulate the flow of nanofluids past a cylindrical device with convective heat transfer. A key finding of their study was that increasing the values of the thermophoresis parameter led to a significant increase in nanoparticle (NP) concentration.

In the field of fluid dynamics, the Casson model provides a useful framework for understanding the flow characteristics of non-Newtonian fluids, such as blood and certain biological fluids [6]. The Casson fluid model, a rheological model, was first introduced by Casson [7]. Malik et al. [8] studied the heat transfer and boundary layer flow of a Casson nanofluid over a vertical cylinder and found that the velocity profile decreased as the Casson fluid parameter increased. Hayath et al. [9] explored the effects of thermal conductivity and changing viscosity properties in magnetohydrodynamic non-Newtonian nanofluid flow. Their study highlighted the importance of the Dufour and Soret effects on the boundary layer flow of the nanofluid. They observed that a decrease in the Soret number and an increase in the Dufour number resulted in significant heating, flow acceleration, and higher temperature magnitudes. Mabood et al. [10] studied the steady forced convection boundary layer nanofluid flow over a horizontal circular cylinder and found that the convective heat transfer coefficient and the solid volume fraction of NPs were related to the enhancement of heat transfer. Hayat et al. [11] examined the Casson fluid boundary layer flow induced by a stretching cylinder in the presence of both heat radiation and NPs. They observed a significant decrease in temperature with an increase in the intensity of Brownian motion. However, with higher Brownian motion parameter values, both the heat transfer rate and the NP concentration at the surface increased. Makkar et al. [12] conducted a mathematical analysis of an unstable boundary layer flow involving a Casson nanofluid in the context of a chemical reaction near a stretching sheet. They found that as the value of the instability parameter increased, the velocity distribution decreased very slowly. Pandey and Kumar [13] investigated the combined

effects of slip boundary conditions, viscous dissipation, and thermal radiation on a Cu-water nanofluid induced by a stretching cylinder in a porous medium. Their findings indicated that the Nusselt number decreased when the thermal slip parameter, radiation parameter, and Eckert number increased. Furthermore, they found that natural convection characteristics and higher velocity slip were used to accelerate the flow. Basha et al. [14] explored the impact of the nonlinear Boussinesq approximation on the entropy generation and fluid transfer properties of a tangent hyperbolic nano-liquid flowing through a horizontal cylinder. Their findings indicated that an increase in the combined convection parameter led to an increase in nanofluid velocity, while higher values of the dimensionless temperature ratio parameter resulted in increased total entropy generation. Ishak et al. [15] proposed a computational solution for the flow and heat transfer around a stretched permeable cylinder. They found that the skin friction coefficient increased with the Reynolds number but remained constant with the Prandtl number. Mukhopadhyay et al. [16] examined the boundary-layer controlled convective motion of a Casson fluid over a symmetric wedge. They discovered that increasing the Casson fluid parameter allowed for control of flow separation. Abo-Dahab et al. [17] elucidated the thermophysical characteristics of viscoelastic fluid flow induced by a nonlinearly stretched surface. They observed that as the chemical reaction progressed, the temperature increased while the NP concentration decreased. Murthy et al. [18] investigated the magnetohydrodynamic boundary layer slip flow of a Casson fluid over a moving cylinder. They noted that an increase in the Hartmann number corresponded to an increase in the skin friction coefficient. Mahdy [19] presented numerical solutions for the flow and heat transfer of a non-Newtonian fluid over a stretched permeable cylinder, considering suction or blowing and the Soret and Dufour effects. They demonstrated that increasing the Casson factor reduced velocity while raised temperature. Moreover, an increase in the Soret parameter and a decrease in the Dufour parameter resulted in a drop in both temperature and concentration.

Casson nanofluids exhibit unique behaviors when subjected to a magnetic field due to the interactions between the suspended NPs and the applied magnetic field [20]. Numerous researchers have incorporated the magnetic field into their studies. Alwawi et al. [21] investigated the natural convection of a Casson nanofluid around a horizontal rotating cylinder in the presence of a magnetic field. They found that the Casson nanofluid with ethylene glycol and copper oxide exhibited the highest temperature and the lowest local Nusselt number. Ogunseye et al. [22] focused on the numerical analysis of a Casson–Williamson reacting nanofluid species in a moving vertical medium. They discovered that the magnetic field increased the material viscosity and the NP thermal conductivity, while the Lewis number enhanced the fluid viscoplasticity. Nabwey et al. [23] studied heat transfer in the combined bioconvection flow of a Carreau nanofluid over an inclined stretchable cylinder subjected to a binary chemical reaction and a varying magnetic field effect. They found that for larger values of the activation energy limit, the

NP concentration in the nanofluid showed an increasing trend. In the presence of magnetic NPs, Walelign et al. [24] developed a mathematical model for the heat and mass transfer in a Casson fluid flow over an inclined stretching cylinder. They found that increasing the non-Newtonian Casson parameter improved the concentration and temperature profiles while decreased the flow velocity. Hamarsheh et al. [25] investigated the effects of NP volume fraction, magnetic force, and Casson parameter on natural convection in the boundary layer region of a horizontal cylindrical structure immersed in a Casson nanofluid with constant heat flux boundary condition. They demonstrated that increasing the Casson parameter reduced temperature, local skin friction, and velocity while increasing the local Nusselt number. Alwawi et al. [20] established a numerical simulation of kerosene oil flowing around a cylindrical form in the presence of an applied magnetic field. They found that the velocity distribution, rate of energy transmission, and skin friction were all enhanced by an increase in the mixed convection parameter or the volume percentage of ultrafine particles. Rahman et al. [26] used an extended cylinder to model and examine the irreversibility of Sutterby nanofluid flow. The data demonstrated that increasing the Forchheimer and porosity factors reduced the velocity field. The velocity and temperature curves revealed a trend that was contrary to the magnetic parameter. A higher Schmidt number was associated with a decline in the concentration distribution.

The study of Casson nanofluid across porous media in lymphatic vessels is a multidisciplinary investigation within the fields of porous media mechanics, fluid dynamics, and biomedical engineering. The objective of this work is to investigate the underlying principles that govern the transport of Casson nanofluid in porous surfaces, with a particular focus on the implications for lymphatic vessel dynamics. Through theoretical analyses and computational simulations we aim to clarify the processes that govern the interaction between Casson nanofluid and porous tissues comprise lymphatic vessels.

2. MATERIALS AND METHODS

2.1 Mathematical Model

Consider a Casson nanofluid flow through a biological tissue comprises an inclined circular cylindrical lymph vessel of radius R and an angle α. In addition, consider a homogeneous magnetic field acts radially with constant intensity B_0, see **Figure 1**.

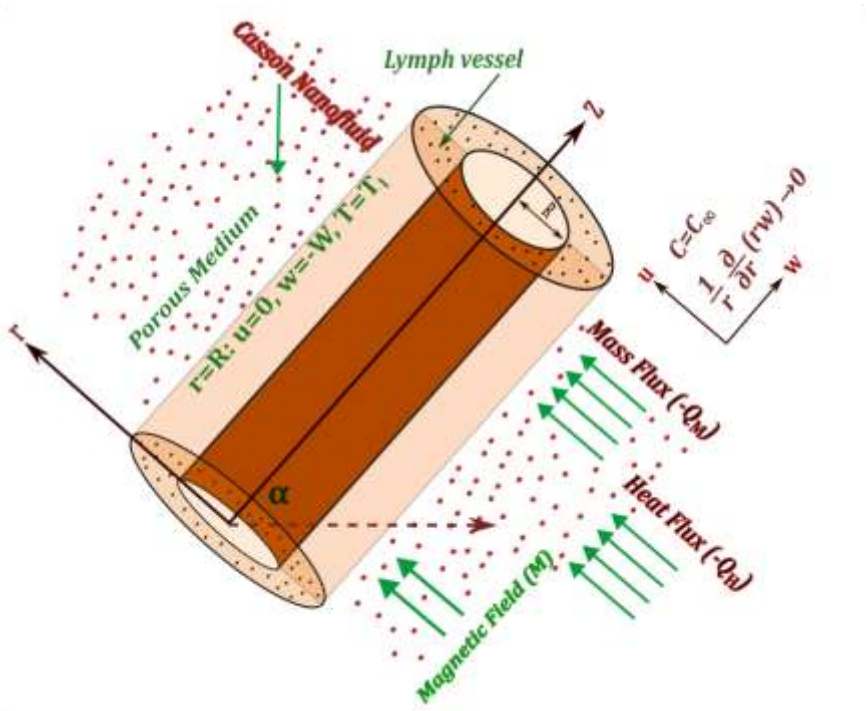

Figure 1: The physical domain for the problem.

By considering the effects of Casson nanofluid parameter, the curvature of the cylinder, the inclination angle, the thermal radiation, and the external magnetic field, we introduce the governing equations for the linear momentum, the mass conservation, thermal energy, and NP concentration in the form [27], [28], [29]:

$$\frac{\partial u}{\partial z}+\frac{\partial w}{\partial r}+\frac{w}{r}=0, \tag{1}$$

$$\frac{1}{\varepsilon^2}\left(u\frac{\partial u}{\partial z}+w\frac{\partial u}{\partial r}\right)=\frac{\upsilon}{\varepsilon}\left(1+\frac{1}{\beta}\right)\left(\frac{\partial^2 u}{\partial r^2}+\frac{1}{r}\frac{\partial u}{\partial r}\right)+\left[\beta_T(T-T_l)+\beta_C(C-C_l)\right]g\cos\alpha-\frac{\sigma B_0^2}{\rho}u-\frac{\upsilon}{K}u, \tag{2}$$

$$u\frac{\partial T}{\partial z}+w\frac{\partial T}{\partial r}=\left(\alpha_f+\frac{16\sigma^* T_\infty^3}{3k^*(\rho c_p)}\right)\left(\frac{\partial^2 T}{\partial r^2}+\frac{1}{r}\frac{\partial T}{\partial r}\right)+\tau\left(\frac{D_B}{\rho_p}\frac{\partial T}{\partial r}\frac{\partial C}{\partial r}+\frac{D_T}{T_\infty}\left(\frac{\partial T}{\partial r}\right)^2\right)+\frac{\upsilon}{c_p}\left(1+\frac{1}{\beta}\right)\left(\frac{\partial u}{\partial r}\right)^2+\frac{\sigma B_0^2}{(\rho c_p)}u^2, \tag{3}$$

$$u\frac{\partial C}{\partial z}+w\frac{\partial C}{\partial r}=D_B\left(\frac{\partial^2 C}{\partial r^2}+\frac{1}{r}\frac{\partial C}{\partial r}\right)+\frac{\rho_p D_T}{T_\infty}\left(\frac{\partial^2 T}{\partial r^2}+\frac{1}{r}\frac{\partial T}{\partial r}\right). \tag{4}$$

Here, (u, w) are fluid velocity components throughout the axial and radial axes of the cylinder respectively, ε is the medium porosity, the NP concentration inside and outside the lymphatic vessel are denoted by C_l and C respectively, υ is the kinematic viscosity, K represents the permeability of the porous medium, β is the Casson parameter, β_c is the volumetric concentration coefficient, β_T thermal expansion coefficient, $\alpha_f = \frac{k_f}{(\rho c_p)_f}$ is the thermal diffusivity, $\tau = \frac{(\rho c_p)_{eff}}{(\rho c_p)_f}$ is the heat capacities ratio of Casson nanofluid and the base fluid, and k^* is the thermal absorption coefficient.

The suitable boundary conditions for the problem are provided by, see [27] and [28]:

$$\text{at } r = R: u = 0, w = -W, \quad T = T_l, \frac{1}{\varepsilon} wC - D_B \frac{\partial C}{\partial r} - \frac{\rho_p D_T}{T_\infty} \frac{\partial T}{\partial r} \to -Q_M , \tag{5}$$

$$\text{as } r \to \infty: \frac{1}{r} \frac{\partial}{\partial r}(rw) \to 0 , C = C_\infty, wT - \left(\alpha_{eff} + \frac{16\sigma^* T_\infty^3}{3k^* (\rho c_p)_{eff}} \right) \frac{\partial T}{\partial r} \to -Q_H . \tag{6}$$

where Q_H denotes the heat flux at the tissue edge interface and Q_M is the NP mass flux at the tissue lymph interface.

The Local Nusselt number Nu is defined as:

$$Nu = \frac{z Q_{HL}}{k(T_l - T_\infty)} , \tag{7}$$

where Q_{HL} is heat flux at the surface of the cylinder.

$$Q_{HL}|_{r=R} = -\left(k + \frac{16\sigma^* T_\infty^3}{3(\rho c_p) k^*} \right) \left[\frac{dT}{dr} \right]_{r=R} .$$

The similarity transformations are presented as:

$$\eta = \sqrt{\frac{\upsilon U_0}{L}} \left(\frac{r^2 - R^2}{2R} \right), u = \frac{U_0 z}{L} F'(\eta), \quad w = \frac{-R}{r} \sqrt{\frac{\upsilon U_0}{L}} F(\eta), \tag{8}$$

$$\theta(\eta) = \frac{T - T_l}{T_\infty - T_l}, \phi(\eta) = \frac{C - C_l}{C_\infty - C_l}$$

Utilizing the non-dimensional transformations Eq. **(8)**, the system of non-dimensional equations Eqs. **(2(3,(4)** can be expressed in the following form:

$$\frac{1}{\varepsilon}\left(1+\frac{1}{\beta}\right)[(1+2\Omega\eta)\mathrm{F}'''+2\Omega\mathrm{F}'']+\frac{1}{\varepsilon^2}\left(\mathrm{FF}''-\mathrm{F}'^2\right)-\mathrm{MF}'-\mathrm{PF}' \\ -(\mathrm{G_r}\theta+\mathrm{G_m}\phi)\cos(\alpha)=0, \tag{9}$$

$$+\frac{1}{\mathrm{P_r}}\left(1+\frac{4}{3}\mathrm{R_d}\right)[(1+2\Omega\eta)\theta''+2\Omega\theta']-\left(1+\frac{1}{\beta}\right)(1+2\Omega\eta)\mathrm{EcF}''^2 \\ -(1+2\Omega\eta)\left(\mathrm{N_t}\theta'^2+\mathrm{N_b}\theta'\phi'\right)-\mathrm{MEcF}'^2+\mathrm{F}\theta'=0, \tag{10}$$

$$(1+2\Omega\eta)\phi''+2\Omega\phi'+\frac{\mathrm{N_t}}{\mathrm{N_b}}\left((1+2\Omega\eta)\theta''+2\Omega\theta'\right)+\mathrm{ScF}\phi'=0. \tag{11}$$

Where: $\Omega=\sqrt{\frac{\upsilon L}{R^2U_0}}$ is the cylinder curvature parameter, $(1+2\Omega\eta)=\frac{r^2}{R^2}$, $M=\frac{\sigma {B_0}^2 L}{\rho U_0}$ is the magnetic field parameter, $P=\frac{\upsilon L}{KU_0}$ is the porosity parameter, $G_r=\frac{g\beta_T(T_l-T_\infty)L^2}{z{U_0}^2}$ is the thermal Grashof number, $G_m=\frac{g\beta_c(C_l-C_\infty)L^2}{z{U_0}^2}$ is the mass Grashof number, $Ec=\frac{{U_w}^2}{(C_p)_f(T_l-T_\infty)}=\frac{{U_0}^2z^2}{(C_p)_f(T_l-T_\infty)L^2}$ is the Eckert number, $\mathrm{P_r}=\frac{\upsilon}{\alpha_f}$ is the Prandtl number, $R_d=\frac{4\sigma^*{T_\infty}^3}{k^*k_f}$ is the radiation parameter, $k_f=\alpha_f\left(\rho C_p\right)$ is the thermal conductivity, $N_t=\frac{\tau D_T(T_l-T_\infty)}{\upsilon T_\infty}$ is the thermophoresis parameter, $N_b=\frac{\tau D_B(C_l-C_\infty)}{\upsilon\rho_p}$ is the Brownian motion parameter, and finally $Sc=\frac{\upsilon}{D_B}$ is the Schmidt number.

The boundary conditions Eqs. **((5,(6)** are also converted into:

$$\text{At }\eta=0\text{: }\mathrm{F}=\gamma,\mathrm{F}'=0,\theta=0,\frac{\mathrm{Sc}}{\varepsilon}(\phi-\xi_1)\mathrm{F}+\phi'+\frac{\mathrm{N_t}}{\mathrm{N_b}}\theta'=-\mathrm{ScQ_M}^*, \tag{12}$$

$$\text{As }\eta\to\infty\text{: }\mathrm{F}'=0,\phi=1,\ \mathrm{P_r}\ (1+2\Omega\eta_\infty)^{-0.5}(\theta-\xi_2)\mathrm{F}+\left(1+\tfrac{4}{3}\mathrm{R_d}\right)(1+ \\ 2\Omega\eta_\infty)^{0.5}\theta'=-\mathrm{P_rQ_H}^*. \tag{13}$$

Where:

$$\gamma=\mathrm{W}\sqrt{\frac{\mathrm{L}}{\upsilon\mathrm{U_0}}},\xi_1=\frac{\mathrm{C_l}}{\mathrm{C_l}-\mathrm{C_\infty}},\mathrm{Q_M}^*=\frac{1}{(\mathrm{C_l}-\mathrm{C_\infty})}\sqrt{\frac{\mathrm{L}}{\upsilon\mathrm{U_0}}}\mathrm{Q_M},\xi_2=\frac{\mathrm{T_\infty}}{\mathrm{T_l}-\mathrm{T_\infty}},\mathrm{Q_H}^*= \\ \frac{1}{(\mathrm{T_l}-\mathrm{T_\infty})}\sqrt{\frac{\mathrm{L}}{\upsilon\mathrm{U_0}}}\mathrm{Q_H}. \tag{14}$$

The non-dimensional Local Nusselt number Nu is defined by:

$$Nu(Re_z)^{\frac{-1}{2}}=-\left(1+\frac{4}{3}R_d\right)\theta'(0)\,.$$

2.2 Numerical Method and Validation

In this section, we used MATLAB to conduct numerical simulations that produced both graphical and numerical results for the flow of a Casson nanofluid. We considered the effects of several crucial factors in these simulations.

2.2.1 Numerical procedure of solution.

We employed the MATLAB function Bvp4c to numerically solve the modified partial differential equations Eqs. **((9,(10(11)** along with the boundary conditions Eqs. **((12(13)**. It was necessary to transform the system of ordinary differential equations (ODEs) into a corresponding system of first-order ODEs. The equations Eqs. **((9,(10(11)** can be expressed as follows:

$$F''' = \frac{-\varepsilon}{(1+2\Omega\eta)\left(1+\frac{1}{\beta}\right)}\left[\frac{2\Omega}{\varepsilon}\left(1+\frac{1}{\beta}\right)F'' + \frac{1}{\varepsilon^2}\left(FF'' - F'^2\right) - MF' - PF' - (G_r\theta + G_m\phi)\cos(\alpha)\right], \tag{15}$$

$$\theta'' = \frac{-p_r}{\left(1+\frac{4}{3}R_d\right)(1+2\Omega\eta)}\left[\frac{2\Omega}{P_r}\left(1+\frac{4}{3}R_d\right)\theta' - (1+2\Omega\eta)\left(N_t\theta'^2 + N_b\theta'\phi'\right) - MEcF'^2 + F\theta' - \left(1+\frac{1}{\beta}\right)(1+2\Omega\eta)EcF''^2\right], \tag{16}$$

$$\phi'' = \frac{-1}{(1+2\Omega\eta)}\left[2\Omega\phi' + \frac{N_t}{N_b}\left((1+2\Omega\eta)\theta'' + 2\Omega\theta'\right) + ScF\phi'\right]. \tag{17}$$

To convert the system of ODEs into a system of first-order ODEs, we define a new set of variables as follows:

$$s_1 = F, s_2 = F', s_3 = F'', s_4 = \theta, s_5 = \theta', s_6 = \phi, s_7 = \phi'. \tag{18}$$

Substituting Eq. **((18)** into equations Eqs. **((15(16,(17)** yields the following system of seven first-order ODEs:

$$s_1' = s_2,$$

$$s_2' = s_3,$$

$$s_3' = F''' = \frac{-\varepsilon}{(1+2\Omega\eta)\left(1+\frac{1}{\beta}\right)}\left[\frac{2\Omega}{\varepsilon}\left(1+\frac{1}{\beta}\right)s_3 + \frac{1}{\varepsilon^2}(s_1 s_3 - {s_2}^2) - Ms_2 - Ps_2 - (G_r s_4 + G_m s_6)\cos(\alpha)\right],$$

$$s_4' = s_5,$$

$$s_5' = \theta'' = \frac{-p_r}{\left(1+\frac{4}{3}R_d\right)(1+2\Omega\eta)}\left[\frac{2\Omega}{P_r}\left(1+\frac{4}{3}R_d\right)s_5 - (1+2\Omega\eta)(N_t {s_5}^2 + N_b s_5 s_7) - M{Ecs_2}^2 + s_1 s_5 - \left(1+\frac{1}{\beta}\right)(1+2\Omega\eta){Ecs_3}^2\right], \quad (19)$$

$$s_6' = s_7,$$

$$s_7' = \phi'' = \frac{-1}{(1+2\Omega\eta)}\left[2\Omega s_7 + \frac{N_t}{N_b}\left((1+2\Omega\eta)s_5' + 2\Omega s_5\right) + Scs_1 s_7\right].$$

The corresponding boundary conditions Eqs. **((12,(13)** become:

$$\text{At } \eta = 0: s_1 = \gamma, s_2 = 0, s_4 = 0, \frac{Sc}{\varepsilon}(s_6 - \xi_1)s_1 + s_7 + \frac{N_t}{N_b}s_5 = -ScQ_M{}^*, \quad (20)$$

$$\text{As } \eta \to \infty: s_2 = 0, s_6 = 1, P_r\,(1+2\Omega\eta)^{-0.5}(s_4 - \xi_2)s_1 + \left(1+\frac{4}{3}R_d\right)(1+2\Omega\eta)^{0.5}s_5 = -P_r Q_H{}^*. \quad (21)$$

The parameter values used in this investigation are listed in **Table 1**.

Table 1: The parameter values used in this study.

parameter	value	parameter	value	parameter	value
ε	0.1	α	20	G_r	0.2
γ	0.3	β	0.5	G_m	0.3
ξ_1	0.35	Ω	7	N_b	0.2
ξ_2	1.5	M	0.6	N_t	0.3
$Q_M{}^*$	0.0001	P	0.5	P_r	1.3
Ec	0.01	Re	0.1	Sc	5
$Q_H{}^*$	0.0001	R_d	0		

2.2.2 Validation

To ensure the accuracy of our code, we compared our numerical results with the published data corresponding similar nanofluid models [27], [28]. This validation process is crucial for confirming the reliability of our simulations and ensuring that our model accurately represents the physical phenomena under study. Excellent agreement is observed as shown in **Table 2**.

Table 2: The local Nusselt number value comparison for various values of Magnetic field at $\mathbf{N_t}$=0.1, $\mathbf{N_b = 0.2}$, Sc=11, $\mathbf{P_r = 10, \Omega = G_m = G_r = \alpha = R_d = Ec = 0, \beta \to \infty}$.

M	Walelign et. al [27]	Ismaeel et. al [28]	[present]
0.0	1.0000	1.0000	1.000000
0.2	1.0197	1.0197	1.019804
0.5	1.1180	1.1180	1.118034
0.8	1.2605	1.2806	1.280631
1.0	1.4142	1.4142	1.414220

3. RESULTS AND DISCUSSION

The numerical simulations were carried out using the MATLAB function Bvp4c to obtain numerical and graphical representations for the flow properties of the Casson nanofluid, considering the effect of some pertinent factors.

Figure 2 illustrates how the dimensionless constant velocity γ influences velocity, temperature, Nusselt number, and NP concentration profiles. **Figure 2(A)** shows that the nanofluid velocity reaches its peak value in the tissue (as $\eta \to \infty$) and then drops to its lowest value at the lymph wall. Additionally, the velocity decreases as γ increases, due to the increase in fluid suction at the lymphatic wall. The influence of γ on nanofluid temperature is shown in **Figure 2(B)**, where the temperature noticeably increases as γ increases. This elevated temperature might be advantageous for cancer therapy which induce cancer cell death. However, it is critical to equilibrium this against the danger of harming healthy tissue. Furthermore, the temperature drops in the region adjacent to the lymph wall. The NP concentration in **Figure 2(C)** is inversely proportional to γ, where it decreases as γ increases. As a result, there will be less NP accumulation in the tumor as

the lymph sucks up the NPs from the tissue. The NP concentration profile follows the trend of the temperature profile in the tissue, starting high at the tissue and falling as it gets closer to the lymph wall. This makes sense considering there are multiple reasons that a dropping temperature might impact drug concentration. A drop in temperature may reduce the Brownian motion of NPs, which might reduce the NP concentration in the tumor tissue. Treatment results may be compromised if NPs are unable to sufficiently concentrate within the tumor to reach therapeutic payload concentrations. The effect of γ on the Nusselt number is revealed in **Figure 2(D)**. The Nusselt number declines as the value of γ increases, which might suggest that heat transfer across the lymph wall is becoming less efficient.

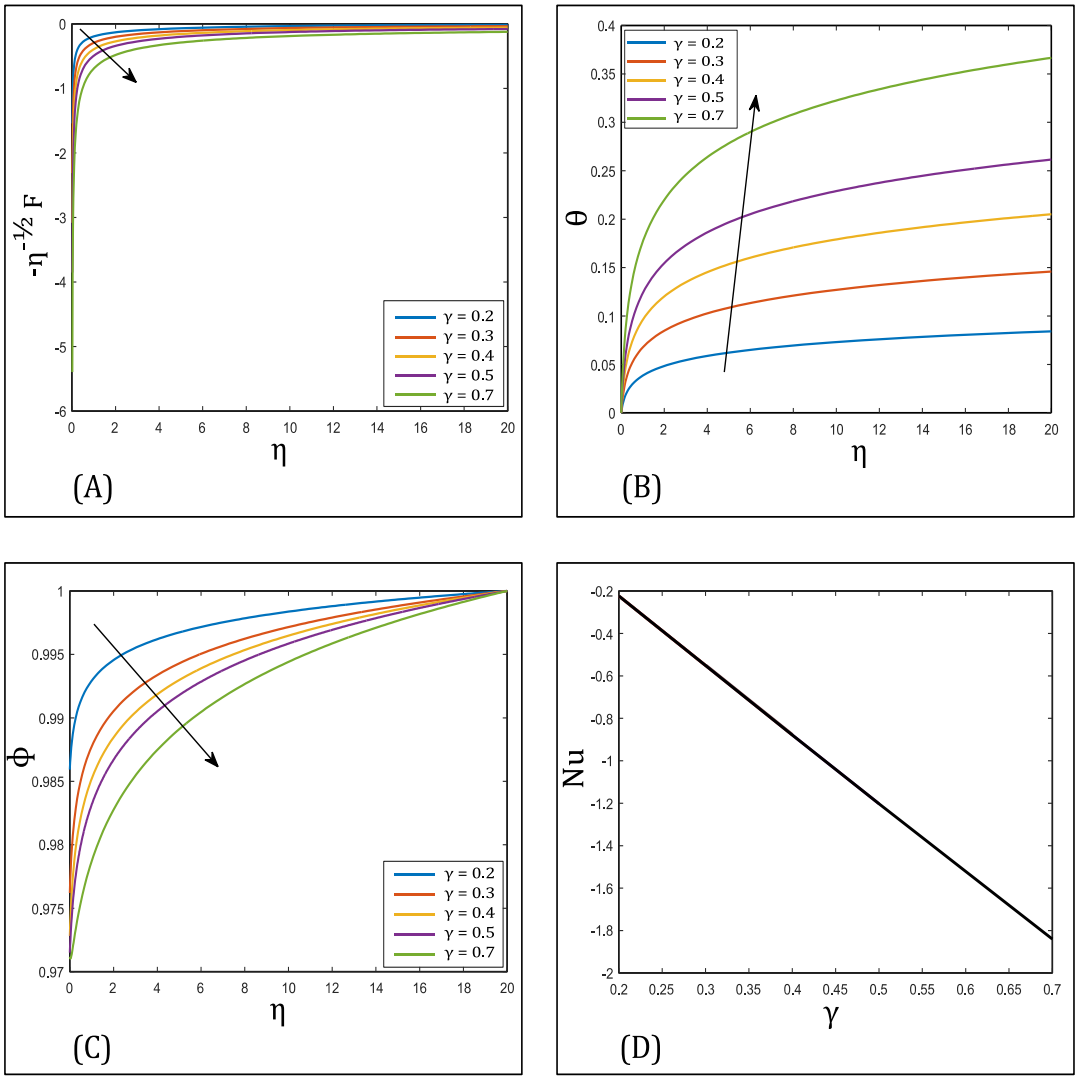

Figure 2: Effect of Dimensionless Constant Parameter **γ** on: (A) The Interstitial Nanofluid Velocity Profile, (B) The Temperature Profile, (C) The NPs Concentration Profile, (D)The Nusselt Number Profile**.**

The effect of the Brownian motion parameter N_b on nanofluid temperature is depicted in **Figure 3(A)**. It is observed that the nanofluid temperature decreases in the case of large N_b values due to the intensified random motion of NPs. **Figure 3(B)** illustrates how N_b affects the concentration of NPs. It is noticed that increasing the N_b values enhances the NP accumulation in the tissue. An increase in the Brownian motion parameter causes the NP concentration to rise as a result of the NPs being more evenly distributed, mixed, and diffused. This shows that the behavior and dispersion of NPs in the tumor are fundamentally governed by Brownian motion. We can see in **Figure 3(C)** that the rate of heat transfer increases as N_b increases.

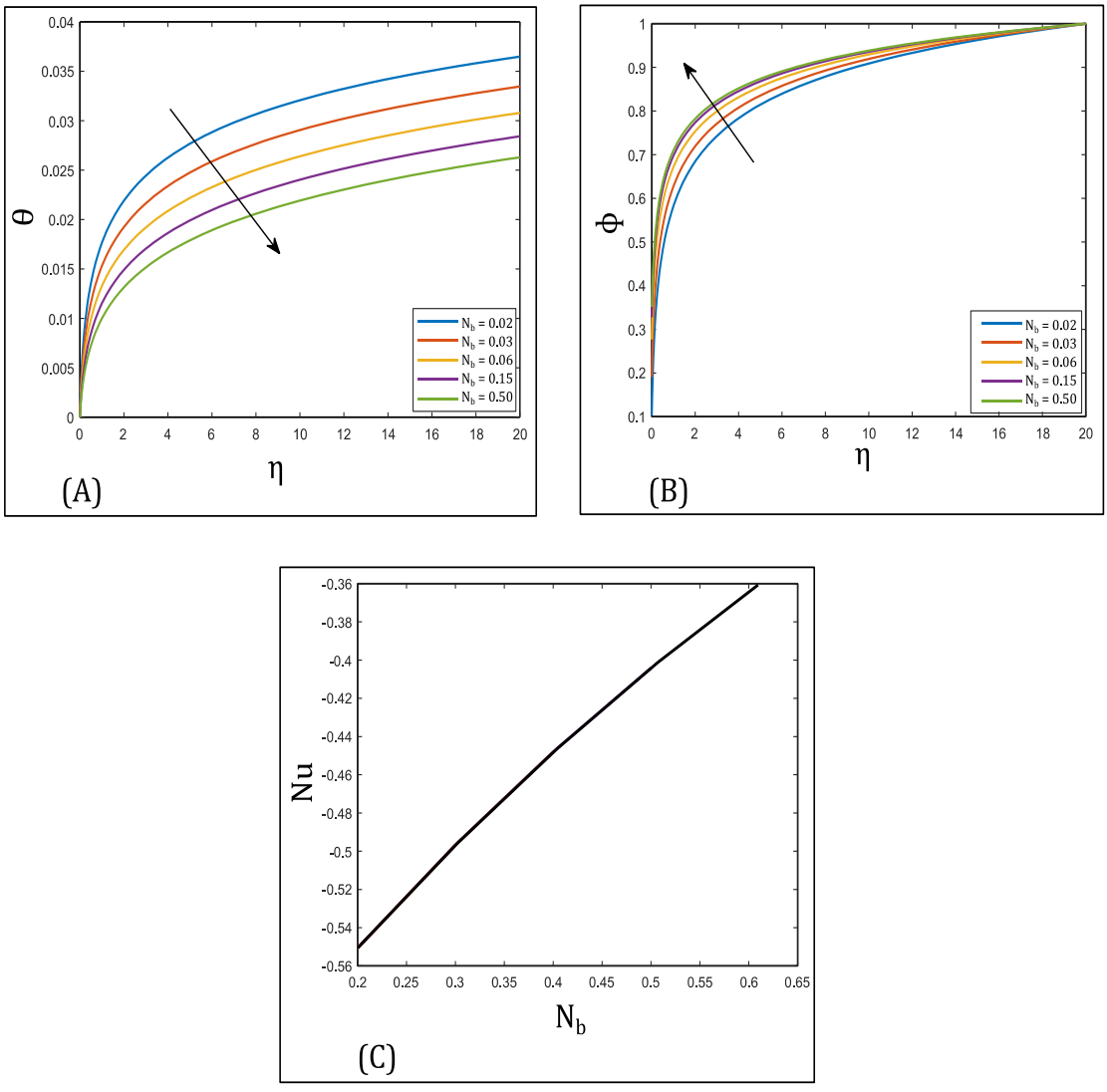

Figure 3: Effect of Brownian Motion Parameter $\mathbf{N_b}$ on: (A) The Temperature Profile, (B) The NPs Concentration Profile, (C)The Nusselt Number Profile.

An essential parameter for analyzing the temperature and NP concentration in nanofluid flow is the thermophoresis parameter N_t. **Figure 4(A-B)** shows how temperature and NP concentration are affected by the thermophoresis parameter N_t. These figures demonstrate that the temperature of the nanofluid decreases with the increase in N_t, and the NP concentration profile exhibits the same tendency. Physically speaking, when N_t increases, the thermophoresis force also increases, tending to transport NPs from hotter to cooler places leading to reducing the fluid temperature as well as the NP concentration. According to the data shown in **Figure 4(C)**, the Nusselt number increases when the thermophoresis parameter N_t increases.

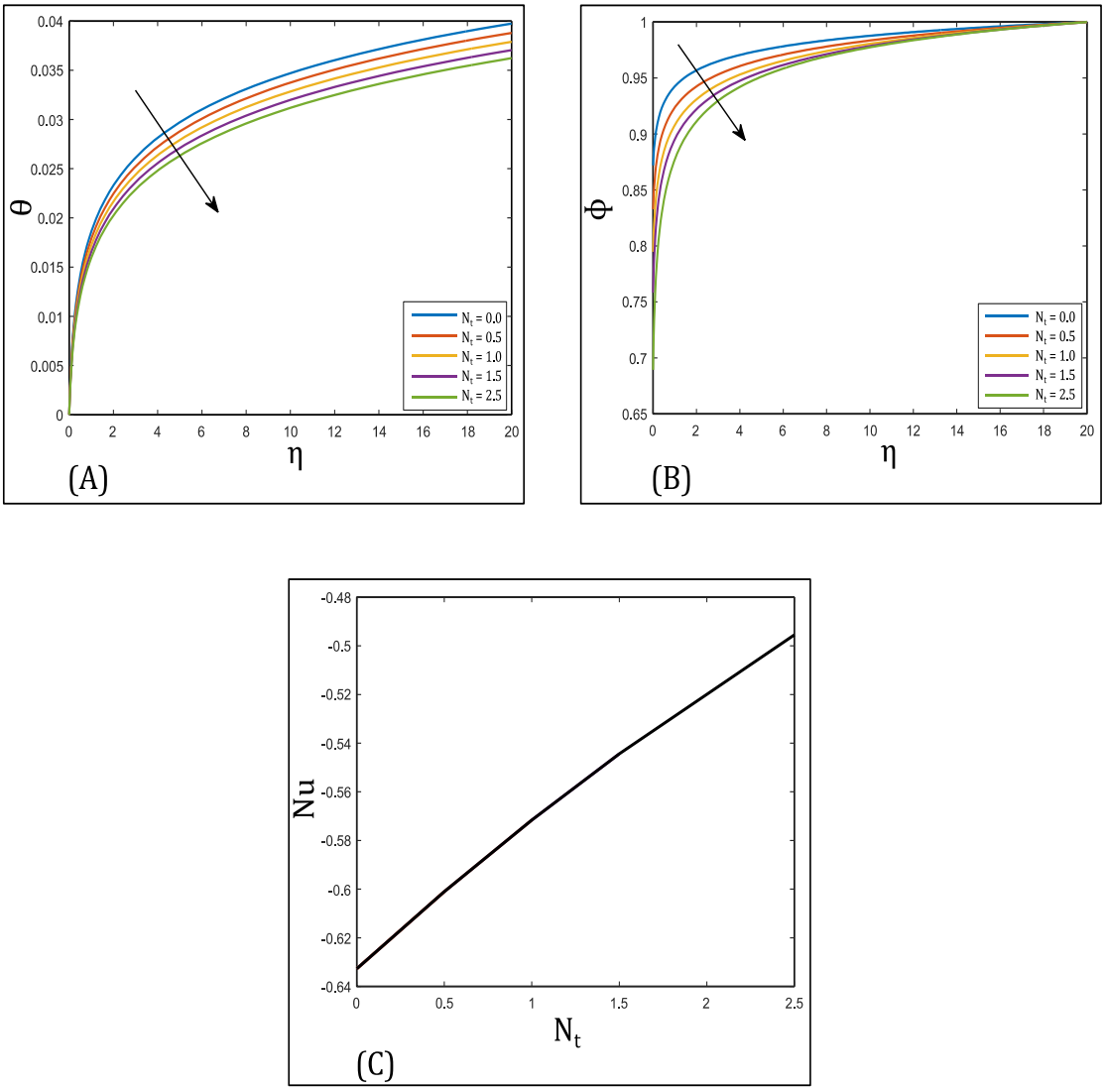

Figure 4: Effect of Thermophoresis Parameter $\mathbf{N_t}$ on: (A) The Temperature Profile, (B) The NPs Concentration Profile, (C)The Nusselt Number Profile.

Figure 5(A-C) illustrates the impact of thermal radiation R_d on the temperature of the nanofluid, the NP concentration, and the Nusselt number. The temperature curve at various R_d values is depicted in **Figure 5(A)**. As R_d increases, the temperature decreases, reaches its maximum value within the tissue, and then drops as it gets closer to the vessel wall. The NP concentration decreases as we approach the vessel wall (at $\eta = 0$). **Figure 5(B)** shows that R_d has a significant impact on the NP concentration profile. The NP concentration profile is seen to increase with increasing levels of thermal radiation. The heat transfer coefficient decreases as R_d increases, as shown in **Figure 5(C)**. Increasing the radiation parameter in thermal therapy facilitates more efficient heat delivery to the tumor, enabling targeted and regulated treatment with little harm to the surrounding healthy tissue.

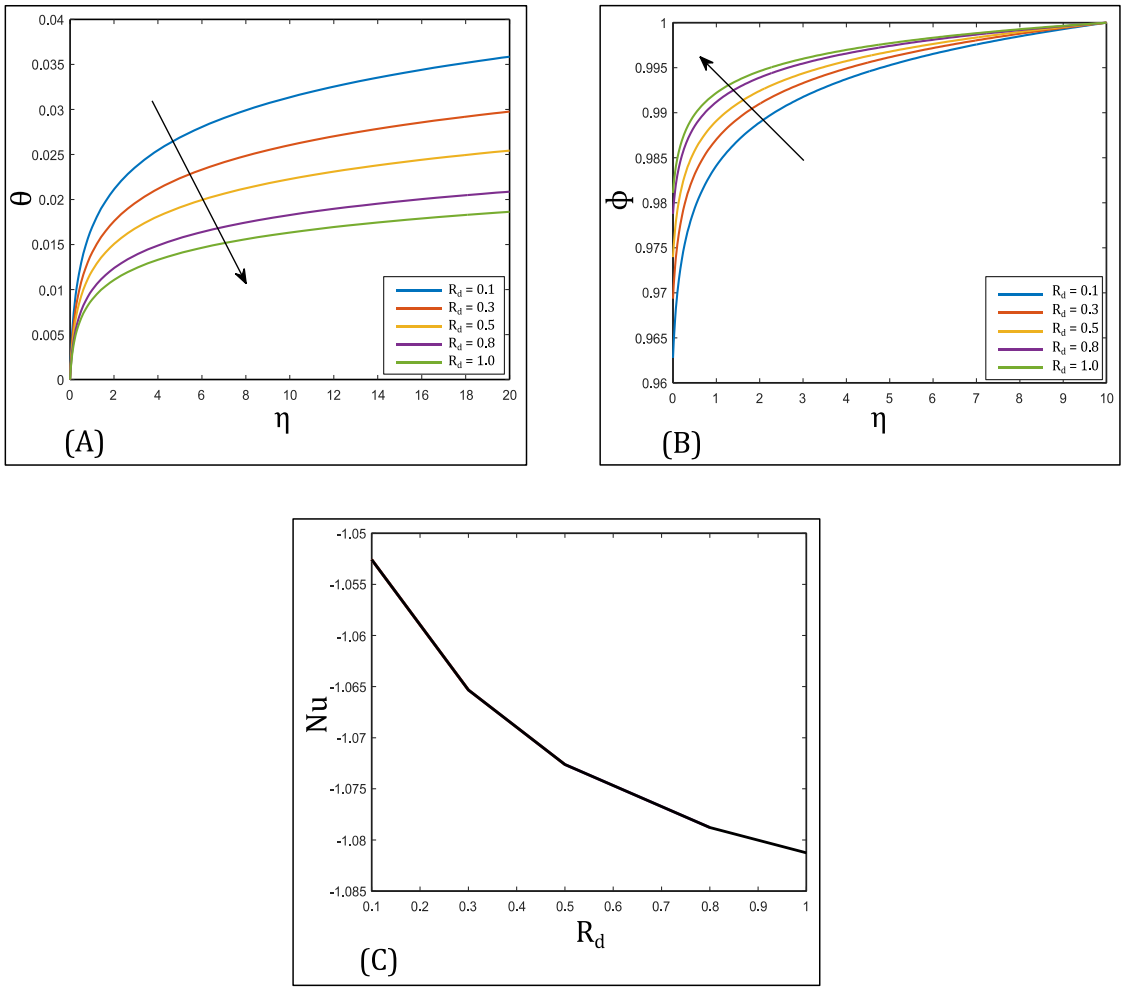

Figure 5: Effect of Radiation parameter $\mathbf{R_d}$ on: (A) The Temperature Profile, (B) The NPs Concentration Profile, (C)The Nusselt Number Profile.

Figure 6(A-C) illustrates the effect of changing the magnetic field parameter M on the temperature of the nanofluid, the concentration of NPs, and the Nusselt number. The graphs clearly show that increasing the magnetic field strength raises the temperature of the nanofluid. This is due to the production of magnetic viscous heating, or additional viscous dissipation, in magnetohydrodynamic flows due to the interaction between the fluid and the magnetic field. Increased magnetic field strength in the system may cause this additional heat output to contribute to an overall temperature increase. Conversely, NP concentration profiles show a declining trend with increasing magnetic field strengths, as seen in **Figure 6(B)**. This is because magnetic viscous heating, which increases thermal energy, can accelerate mixing and diffusion processes, thereby lowering the concentration. The impact of the magnetic field parameter M on the Nusselt number is seen in **Figure 6(C)**, where the Nusselt number decreases as M increases.

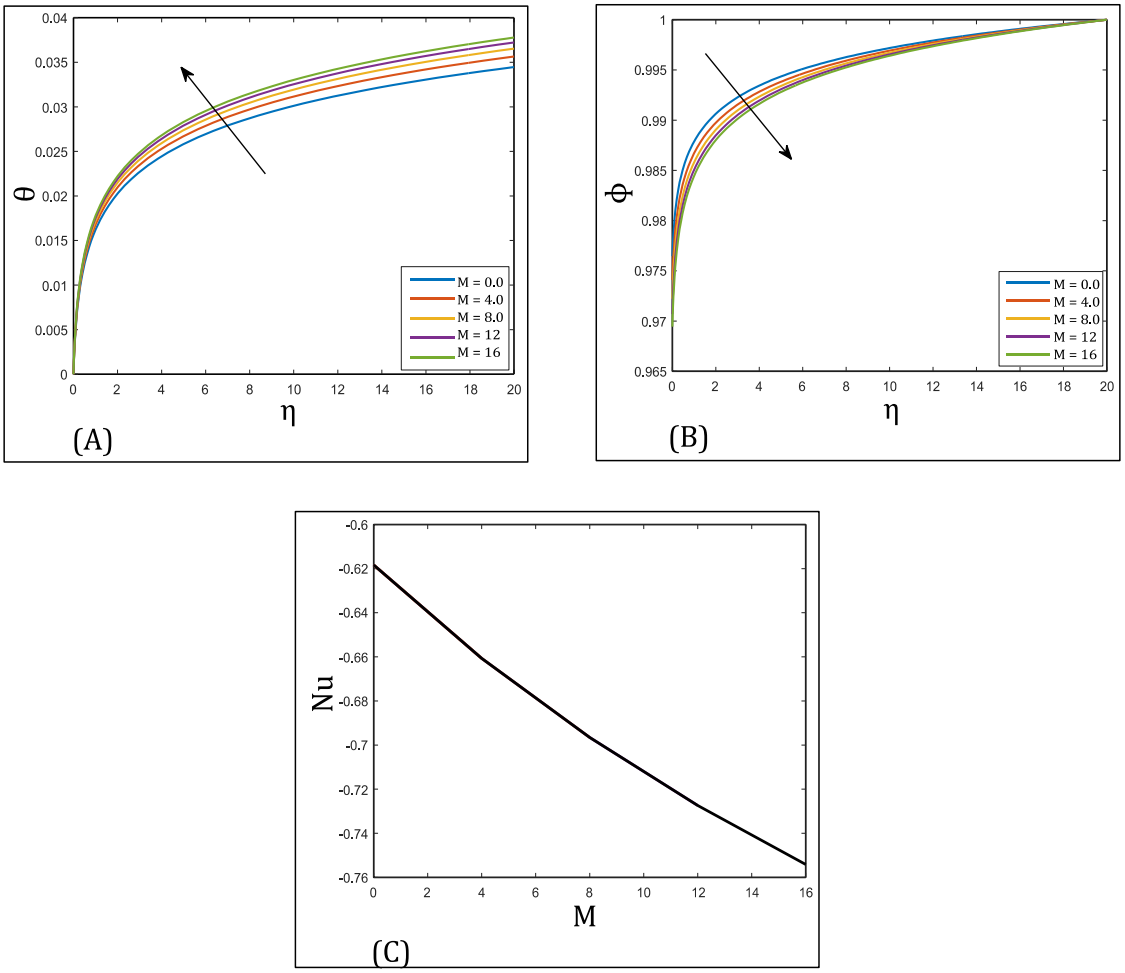

Figure 6: Effect of Magnetic Field Parameter **M** on: (A) The Temperature Profile, (B) The NPs Concentration Profile, (C)The Nusselt Number Profile.

Figure 7(A) depicts the behavior of the nanofluid temperature for different values of the porous medium parameter P. It is observed that as P increases, the temperature of the nanofluid also increases. The NP concentration as a function of η for different values of porous medium parameter P is shown in **Figure 7(B)**. As P increases, the NP concentration decreases. **Figure 7(C)** illustrates that the Nusselt number decreases with an increase in the porous medium parameter P.

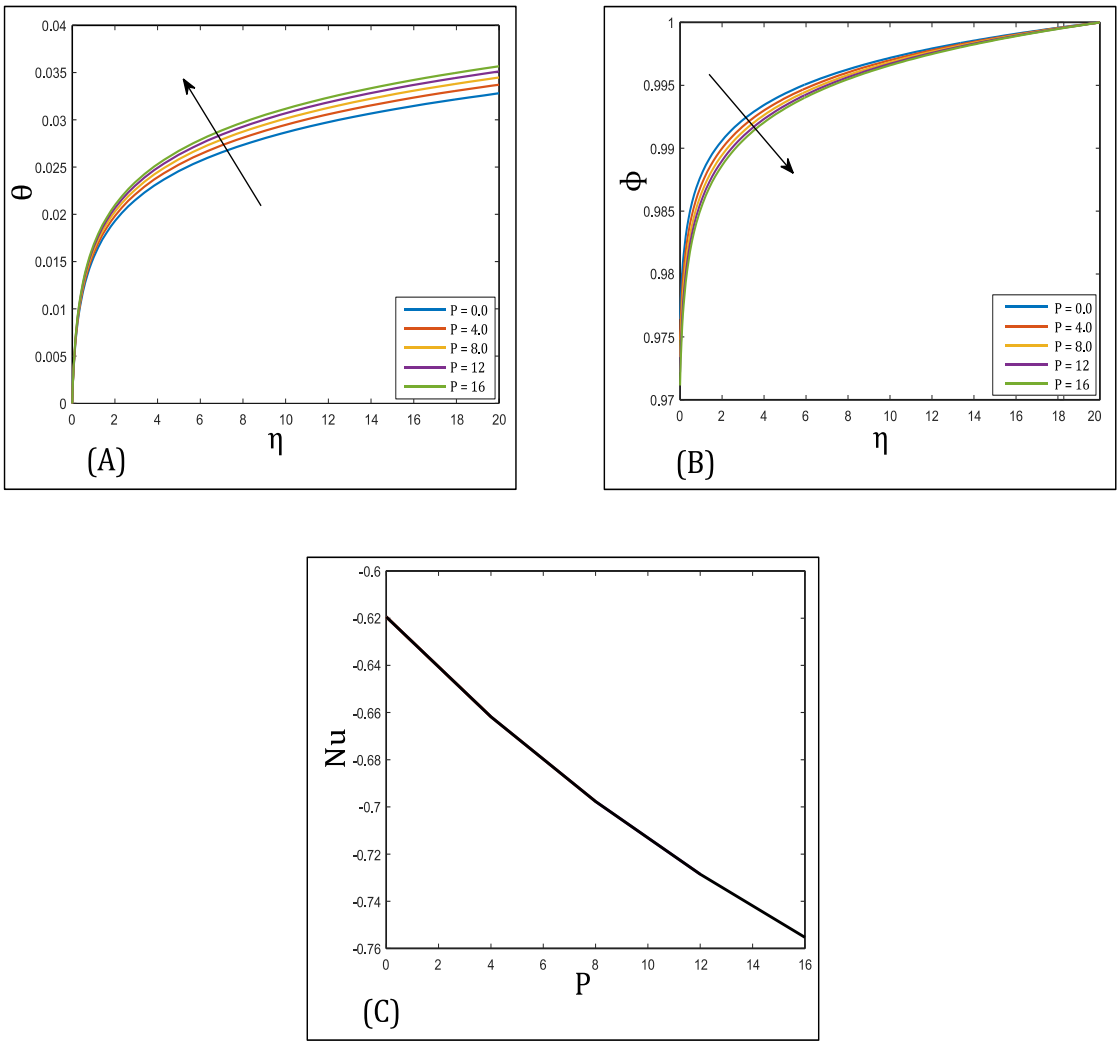

Figure 7: Effect of Porous Medium Parameter **P** on: (A) The Temperature Profile, (B) The NPs Concentration Profile, (C)The Nusselt Number Profile.

The effects of the mass Grashof number G_m on the flow dynamics are examined and illustrated in **Figure 8(A-C)**. Both the NP concentration and the nanofluid temperature decrease as G_m increases. Larger G_m accelerate the cooling process, as revealed in **Figure 8(B)**. Similar to the NP concentration, the nanofluid temperature exhibits a significant initial variation within the tissue before decreasing near the lymph

wall. As shown in **Figure 8(C)**, increasing the values of G_m results in a higher Nusselt number.

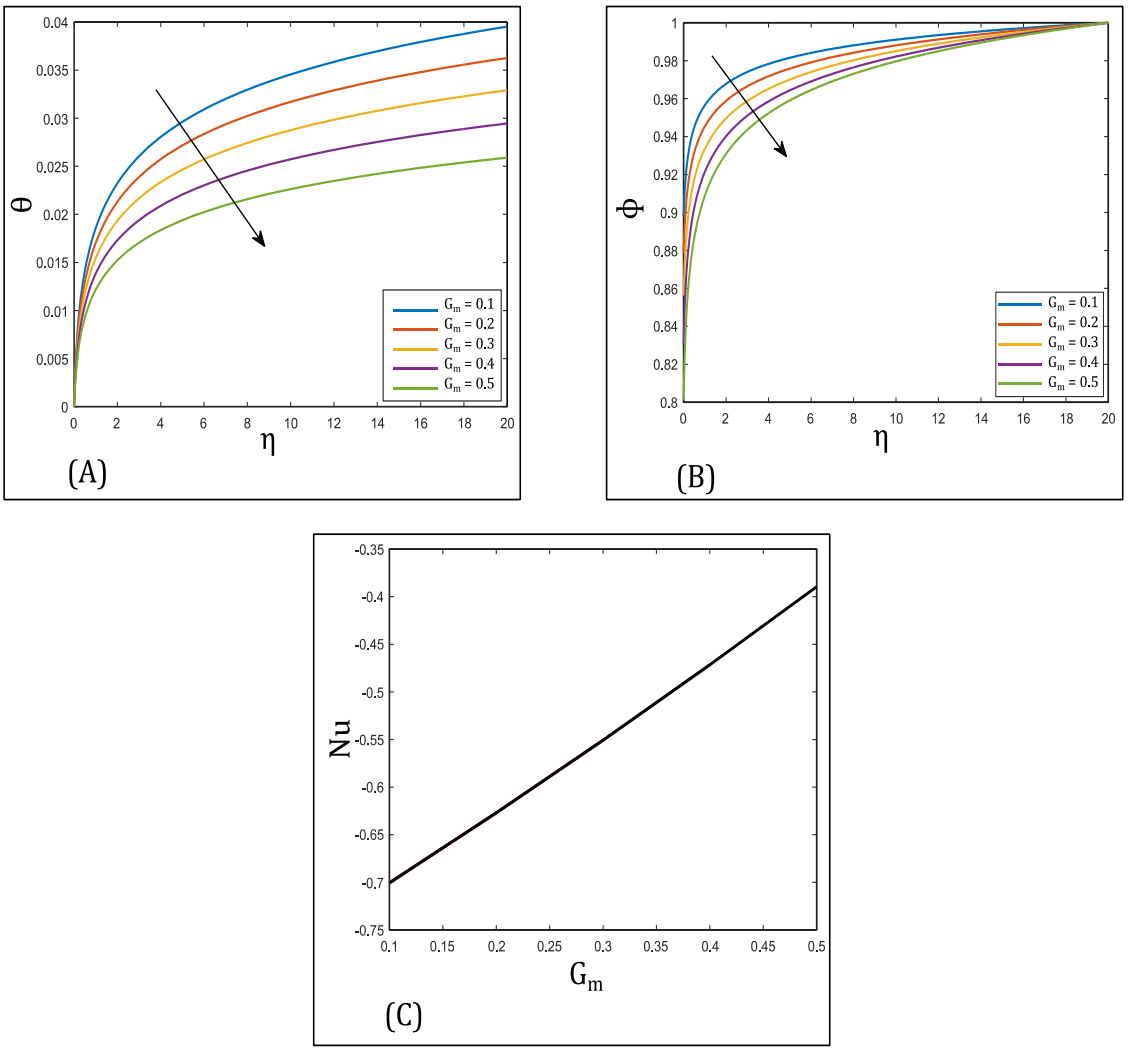

Figure 8: Effect of Mass Grashof Number $\mathbf{G_m}$ on: (A) The Temperature Profile, (B) The NPs Concentration Profile, (C)The Nusselt Number Profile.

Figure 9(A) presents the influence of the thermal Grashof number G_r on the nanofluid temperature. It is observed that as G_r increases, the temperature decreases. The nanofluid temperature drops even if it is in a warm environment because convective heat transfer promotes more efficient cooling. **Figure 9(B)** shows the impact of G_r on the NP concentration. It's clear that the concentration increases with the increase in G_r values. The fluctuation of the Nusselt number with G_r is shown in **Figure 9(C)**. Consequently, when the value of G_r increases, the heat transfer coefficient improves. In thermal therapy applications, this can lead to better treatment outcomes by improving

the dispersion of therapeutic chemicals and delivering heat to the target area more effectively.

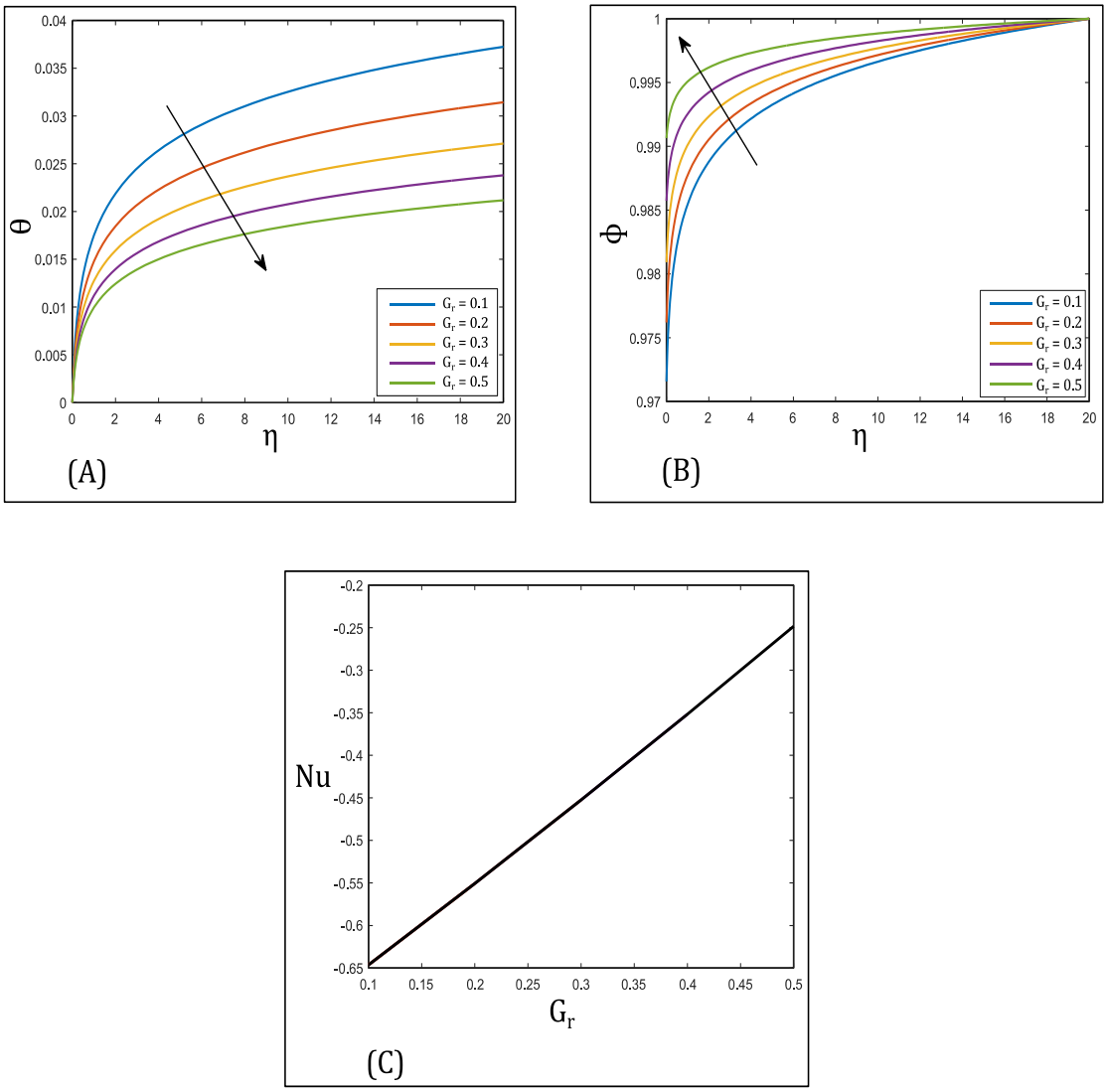

Figure 9: Effect of Thermal Grashof Number $\mathbf{G_r}$ on: (A) The Temperature Profile, (B) The NPs Concentration Profile, (C)The Nusselt Number Profile.

Figure 10(A) depicts the effect of the Eckert number Ec on the nanofluid temperature. It is observed that the nanofluid temperature decreases for large Ec values. **Figure 10(B)** illustrates the influence of Ec on the NP concentrations. It is observed that increasing the Ec values increases the NP concentration in the fluid. In **Figure 10(C)**, we see that as Ec increases, so does the rate of heat transfer rate. This higher heat transfer rate can assist reach and preserve therapeutic temperatures more quickly, resulting in better treatment outcomes. Physically speaking, a higher Eckert number results in a lower

temperature because of improved convective heat transfer and better fluid mixing. It also enhances the concentration of NPs in the fluid. This can result in better heat delivery to the target tissue and better therapeutic agent distribution in thermal therapy applications, both of which can lead to more successful treatment outcomes.

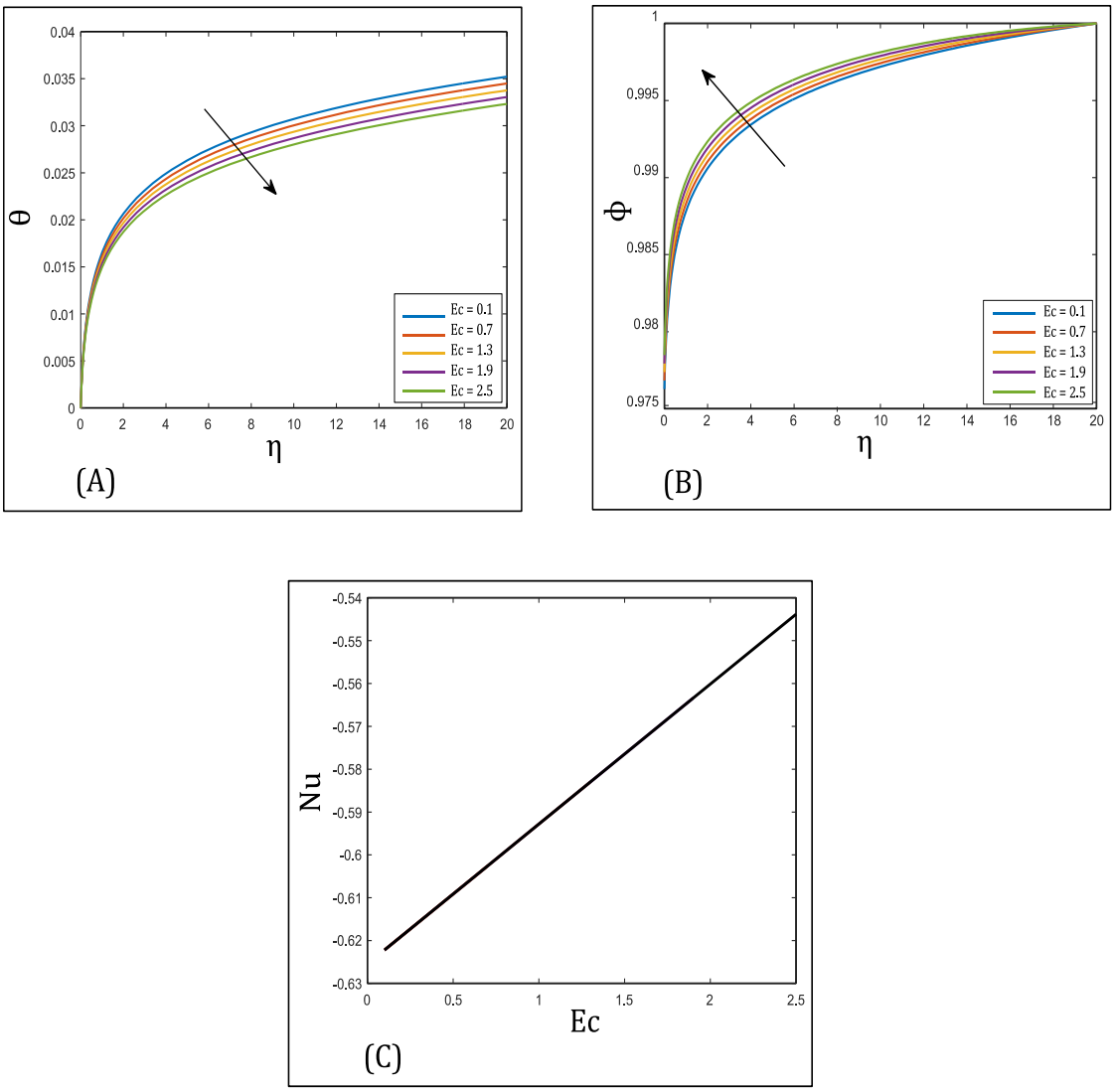

Figure 10: Effect of Eckert Number **Ec** on: (A) The Temperature Profile, (B) The NPs Concentration Profile, (C)The Nusselt Number Profile.

Studying the effects of the cylinder angle of inclination α on flow profiles is essential because it influences the flow dynamics, heat transfer properties, and NP dispersion behavior in nanofluid systems. As shown in **Figure 11(A-B)**, the NP concentration decreases and the nanofluid temperature increases as the cylinder is shifted from a horizontal ($\alpha = 0$) to vertical ($\alpha = \pi/2$) orientation. Variations in the inclination angle can affect the formation and thickness of boundary layers near the cylinder surface,

which in turn impacts the heat transport mechanisms. The impact of the inclination angle α on the Nusselt number is seen in **Figure 11(C)**, where larger α values cause the Nusselt number to decrease.

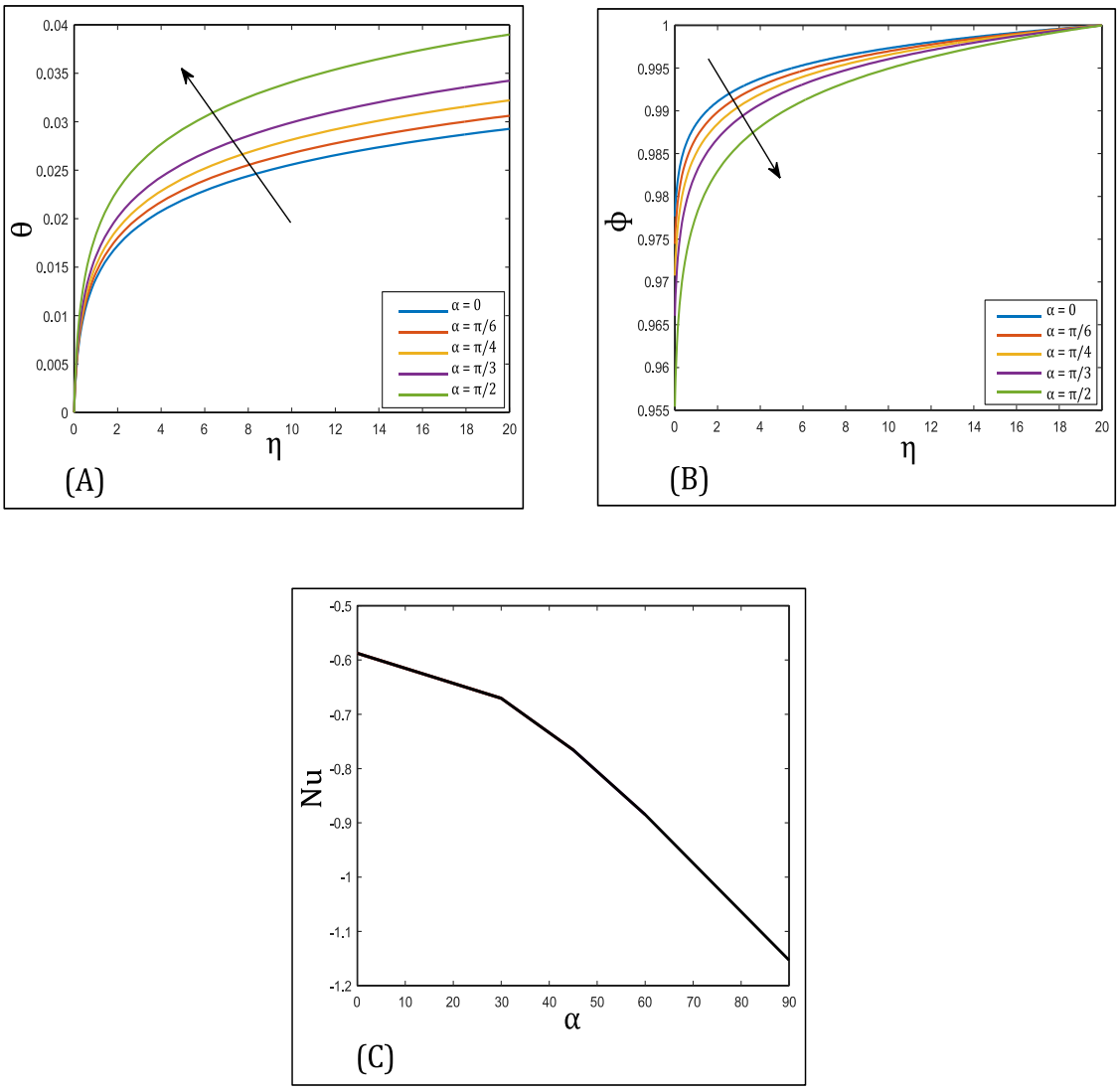

Figure 11: Effect of Inclination Angle **α** on: (A) The Temperature Profile, (B) The NPs Concentration Profile, (C)The Nusselt Number Profile.

Figure 12(A-C) illustrates how the Casson nanofluid parameter β affects the profiles of nanofluid temperature, NP concentration, and Nusselt number. **Figure 12(A-C)** clarifies that while NP concentration and Nusselt number increase, the temperature of the nanofluid decreases as the Casson fluid parameter β increases. The cooling impact occurs because of the Casson fluid parameter, even if thermal conductivity improves with higher NP concentration and Nusselt number. The enhanced Casson fluid parameter

might cause modifications to fluid viscosity or flow patterns that impede heat transmission, lowering the temperature of the nanofluid.

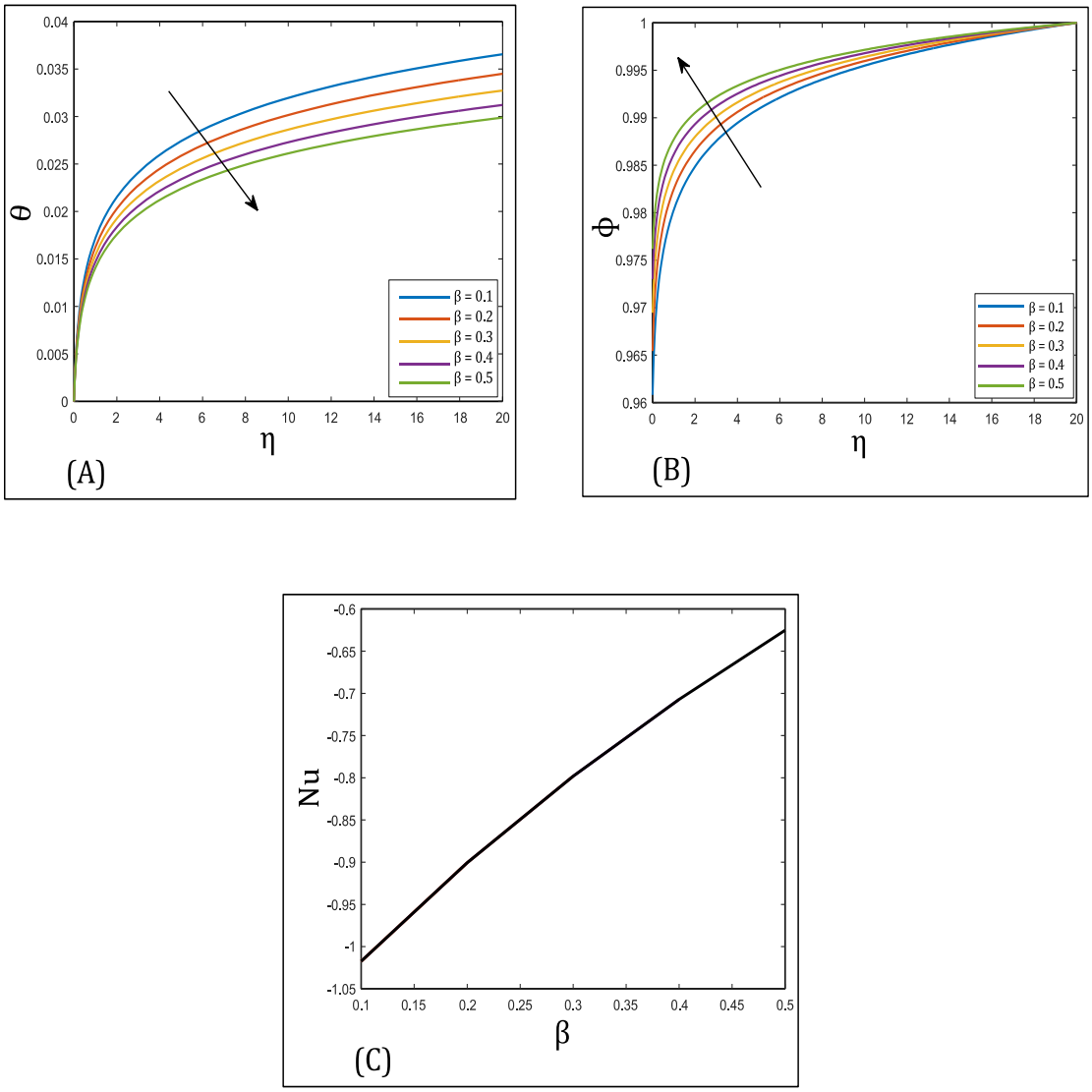

Figure 12: Effect of Casson Parameter **β** on: (A) The Temperature Profile, (B) The NPs Concentration Profile, (C)The Nusselt Number Profile.

The impact of the curvature parameter Ω on the temperature, NP concentration, and Nusselt number profiles is displayed in **Figure 13(A-C)**. **Figure 13(A)** shows the effect of Ω on the temperature of the nanofluid. The relationship between the curvature parameter and the cylinder radius is undoubtedly inverse. As such, the radius of the cylinder tends to decrease as the curvature parameter Ω increases. When this occurs, the cylinder surface area decreases, leading to a drop in the fluid temperature due to an increase in the surface velocity gradient caused by an increase in the curvature parameter

Ω. The temperature rises for a considerable distance away from the wall before falling close to the cylinder wall. The impact of Ω on the concentration of NP is apparent in **Figure 13(B)**. An increase in Ω results in a reduction in NP concentration that reaches its minimal value near the vessel wall. This decrease in concentration can be considered to be due to the drop in temperature, as lower temperature may reduce the potential energy of the NPs. This fall in concentration might also be attributed to NP absorption by the lymph. On the other hand, lymphatic vessels absorb cellular waste, toxins, and NP residue to lymph nodes for filtering and removal. The lymphatic system assists in preserving the health and functionality of tissue by eliminating these waste materials. Furthermore, the Nusselt number at the lymph walls is increasing with the increase in Ω values, as seen in **Figure 13(C)**.

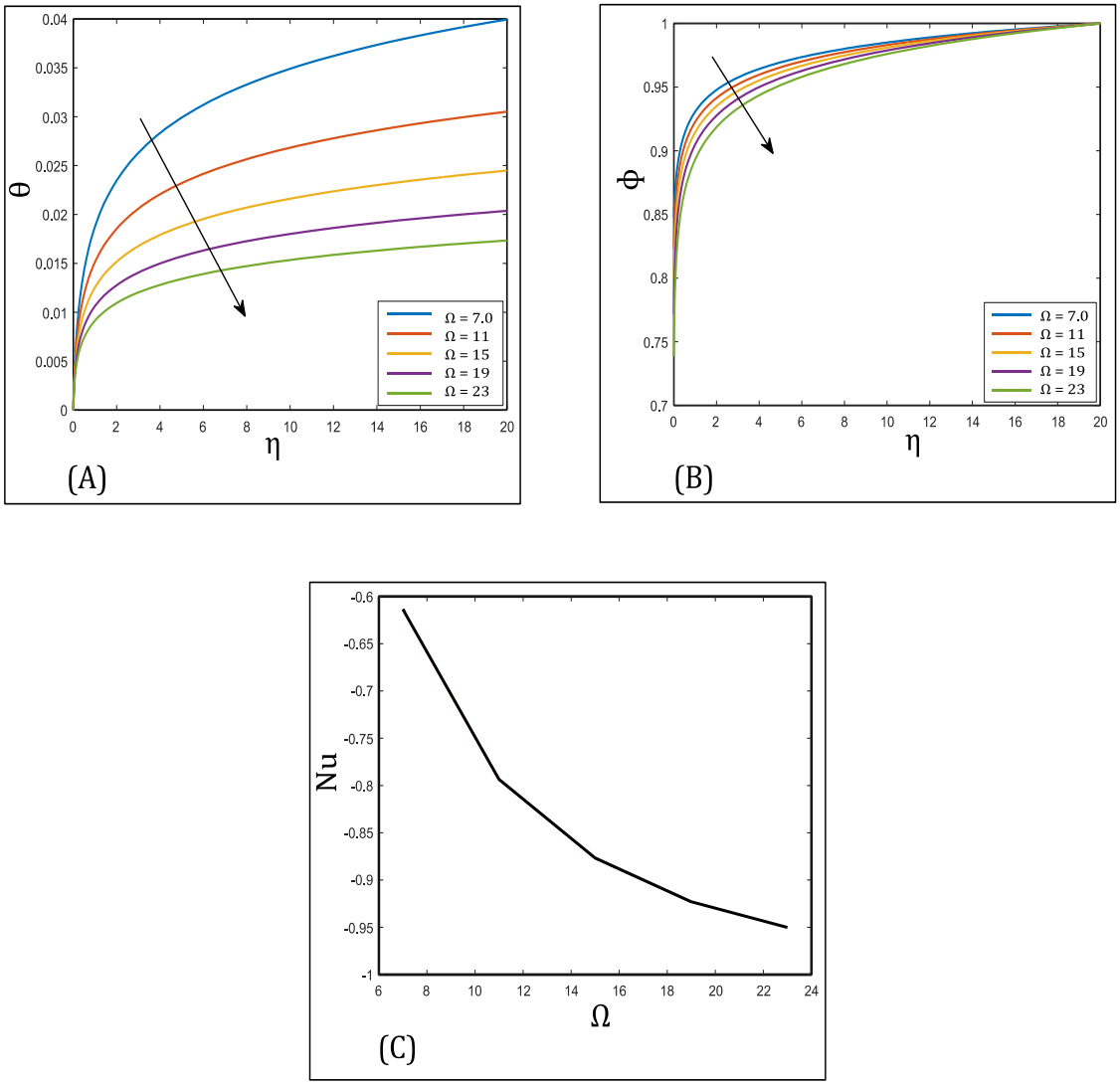

Figure 13: Effect of Cylinder Curvature Parameter **Ω** on: (A) The Temperature Profile, (B) The NPs Concentration Profile, (C)The Nusselt Number Profile.

4. CONCLUSION

This study has explored the mechanisms of heat and mass transfer in the flow of a Casson nanofluid across an inclined circular cylinder subjected to a magnetic field. The governing partial differential equations were transformed into ordinary differential equations using non-dimensional variables. The Bvp4c built in function in MATLAB was employed to provide a numerical solution to the problem dimensionless governing equations. The profiles of temperature, velocity, and NP concentration were graphically demonstrated for various parameter values. The major findings of this investigation are as follows:

- The dimensionless fluid flux parameter significantly influences the interstitial nanofluid velocity. This influence is clearly depicted in the graph and shows a diminishing effect.
- Both the nanofluid temperature and the NP concentration in this flow exhibit a decreasing pattern, peaking in the tissue and subsequently falling near the lymph vessel wall.
- The temperature of the nanofluid increases with the rise in the values of the fluid flux parameter, the magnetic field parameter, the porous medium parameter, the inclination angle, and the thermophoresis parameter. Conversely, it decreases with the rise in the values of the thermal Grashof number, the Eckert number, the mass Grashof number, the Casson parameter, and the curvature parameter.
- The NP concentration can be improved by increasing the thermal Grashof number, Casson parameter, radiation parameter, Eckert number, and Brownian motion parameter. Conversely, it can be reduced by increasing the parameters for the mass Grashof number, inclination angle, curvature, magnetic field, thermophoresis, mass Grashof number, mass, and porous media.
- An increase in the Nusselt number can be achieved by increasing the Brownian motion parameter, thermophoresis parameter, mass Grashof number, thermal Grashof number, Eckert number, and Casson parameter. In contrast, the Nusselt number decreases by increasing the dimensionless constant parameter, radiation parameter, magnetic field parameter, porous medium parameter, inclination angle, or curvature parameter.

These findings provide valuable insights into the dynamics of Casson nanofluid flow across an inclined circular cylinder and can guide future research in this area. Further studies could explore the effects of other parameters and conditions on the flow properties of Casson nanofluids.

List of symbols.

D_B	Brownian diffusion coefficient $[L^2T^{-1}]$
D_T	Thermophoretic diffusion coefficient $[L^2T^{-1}]$
G_m	Mass Grashof number
G_r	Thermal Grashof number
g	Acceleration due to gravity $[\ L\ T^{-2}]$
B_0	External magnetic field $[N\ A^{-1}L^{-1}]$
R_d	Radiation parameter
P_r	Prandtl number
Sc	Schmidt number
N_t	Thermophoresis parameter
N_b	Brownian motion parameter
K	Porous medium permeability
Q_M, Q_H	Mass flux, heat flux respectivly
$Q_M{}^*, Q_H{}^*$	Mass flux coefficient, Heat flux coefficient respectivly
Nu	Nusselt number
M	Magnetic field parameter
T_l	Fluid temperature near the wall [K]
T_∞	Temperature far away from the wall [K]
C_l	Nanoparticle Concentration in the lymph vessel $[Mol\ L^{-3}]$
C_∞	Nanoparticle concentration away from the wall $[Mol\ L^{-3}]$
P	Porosity parameter
Ec	Eckert number
F	Dimensionless Stream function
w, u	Velocity components in r, z directions $[m\ L^{-1}]$
F'	Dimensionless velocity

k_f	Thermal conductivity $[Wm^{-1}K^{-1}]$

Greek symbols

ε	Medium porosity
α	Inclination angle
β	Casson nanofluid parameter
β_T	Thermal expansion coefficient
β_C	Volumetric concentration coefficient
θ, ϕ	Dimensionless temperature and concentration
ξ_1, ξ_2	Dimensionless constants
Ω	Cylinder curvature parameter
γ	Dimensionless constant velocity
υ	Kinematic viscosity $[L^2T^{-1}]$
τ	Heat capacities ratio
(ρc_p)	Heat capacity $[ML^2T^{-2}]$
α_f	Thermal diffusivity $[L^2T^{-1}]$
η	Similarity variable

Subscripts

∞	Ambient conditions
p	Constant pressure
l	Lymph
eff	Effective
f	Nanofluid

Superscripts

$'$	Differentiation with respect to η
*	Dimensionless property

REFERENCES

[1] L. Cheng, "Nanofluid Heat Transfer Technologies," Recent Patents Eng., vol. 3, no. 1, pp. 1–7, 2009, doi: https://doi.org/10.2174/187221209787259875.

[2] A. Albojamal and K. Vafai, "Analysis of particle deposition of nanofluid flow through porous media," Int. J. Heat Mass Transf., vol. 161, p. 120227, 2020, doi: https://doi.org/10.1016/j.ijheatmasstransfer.2020.120227.

[3] S. U. S. Choi and J. A. Eastman, "Enhancing thermal conductivity of fluids with nanoparticles," ASME Int. Mech. Eng. Congr. Expo., pp. 99–105, 1995, doi: https://www.osti.gov/biblio/196525.

[4] J. Buongiorno, "Convective transport in nanofluids," J. Heat Transfer, vol. 128, no. 3, pp. 240–250, 2006, doi: https://doi.org/10.1115/1.2150834.

[5] Hashim, A. Hamid, and M. Khan, "Transient flow and heat transfer mechanism for Williamson-nanomaterials caused by a stretching cylinder with variable thermal conductivity," Microsyst. Technol., vol. 25, no. 9, pp. 3287–3297, 2019, doi: https://doi.org/10.1007/s00542-019-04364-9.

[6] T. Sochi, "Non-newtonian rheology in blood circulation," arXiv Prepr. arXiv, pp. 1–26, 2013, doi: http://arxiv.org/abs/1306.2067.

[7] N. Casson, "Flow equation for Pigment-oil suspensions of the printing ink-type," Rheol. Disperse Syst., pp. 84–104, 1959.

[8] M. Y. Malik, M. Naseer, S. Nadeem, and A. Rehman, "The boundary layer flow of Casson nanofluid over a vertical exponentially stretching cylinder," Appl. Nanosci., vol. 4, no. 7, pp. 869–873, 2014, doi: https://doi.org/10.1007/s13204-013-0267-0.

[9] T. B. Hayath, S. Ramachandran, R. P. Vallampati, and O. A. Bég, "Computation of non-similar solution for magnetic pseudoplastic nanofluid flow over a circular cylinder with variable thermophysical properties and radiative flux," Int. J. Numer. Methods Heat Fluid Flow, vol. 31, no. 5, pp. 1475–1519, 2020, doi: https://doi.org/10.1108/HFF-04-2020-0236.

[10] F. Mabood, W. A. Khan, and M. M. Yovanovich, "Forced convection of nanofluid flow across horizontal circular cylinder with convective boundary condition," J. Mol. Liq., vol. 222, pp. 172–180, 2016, doi: https://doi.org/10.1016/j.molliq.2016.06.086.

[11] T. Hayat, S. Asad, and A. Alsaedi, "Flow of Casson fluid with nanoparticles," Appl. Math. Mech., vol. 37, no. 4, pp. 459–470, 2016, doi: https://doi.org/10.1007/s10483-016-2047-9.

[12] V. Makkar, T. Hayat, and A. Alsaedi, "A mathematical simulation of unsteady MHD Casson nanofluid flow subject to the influence of chemical reaction over a stretching surface: Buongiorno's model," Heat Transf., vol. 50, no. 8, pp. 8640–8655, 2021, doi: https://doi.org/10.1002/htj.22294.

[13] A. K. Pandey and M. Kumar, "Natural convection and thermal radiation influence on nanofluid flow over a stretching cylinder in a porous medium with viscous dissipation," Alexandria Eng. J., vol. 56, no. 1, pp. 55–62, 2017, doi: https://doi.org/10.1016/j.aej.2016.08.035.

[14] H. T. Basha, R. Sivaraj, V. R. Prasad, and O. A. Beg, "Entropy generation of tangent hyperbolic nanofluid flow over a circular cylinder in the presence of nonlinear Boussinesq approximation: a non-similar solution," J. Therm. Anal. Calorim., vol. 143, no. 3, pp. 2273–2289, 2021, doi: https://doi.org/10.1007/s10973-020-09981-5.

[15] A. Ishak, R. Nazar, and I. Pop, "Uniform suction/blowing effect on flow and heat transfer due to a stretching cylinder," Appl. Math. Model., vol. 32, no. 10, pp. 2059–2066, 2008, doi: https://doi.org/10.1016/j.apm.2007.06.036.

[16] S. Mukhopadhyay, I. C. Mondal, and A. J. Chamkha, "Casson fluid flow and heat transfer past a symmetric wedge," Heat Transf. - Asian Res., vol. 42, no. 8, pp. 665–675, 2013, doi: https://doi.org/10.1002/htj.21065.

[17] S. M. Abo-Dahab, M. A. Abdelhafez, F. Mebarek-Oudina, and S. M. Bilal, "MHD Casson nanofluid flow over nonlinearly heated porous medium in presence of extending surface effect with suction/injection," Indian J. Phys., vol. 95, no. 12, pp. 2703–2717, 2021, doi: https://doi.org/10.1007/s12648-020-01923-z.

[18] M. K. Murthy, C. S. K. Raju, V. Nagendramma, S. A. Shehzad, and A. J. Chamkha, "Magnetohydrodynamics boundary layer slip casson fluid flow over a dissipated stretched cylinder," Defect Diffus. Forum, vol. 393, pp. 73–82, 2019, doi: https://doi.org/10.4028/www.scientific.net/DDF.393.73.

[19] A. Mahdy, "Heat transfer and flow of a casson fluid due to a stretching cylinder with the Soret and Dufour Effects," J. Eng. Phys. Thermophys., vol. 88, no. 4, pp. 928–936, 2015, doi: https://doi.org/10.1007/s10891-015-1267-6.

[20] F. A. Alwawi, A. S. Hamarsheh, H. T. Alkasasbeh, and R. Idris, "Mixed convection flow of magnetized Casson nanofluid over a cylindrical surface," Coatings, vol. 12, no. 3, p. 296, 2022, doi: https://doi.org/10.3390/coatings12030296.

[21] F. A. Alwawi, H. T. Alkasasbeh, A. M. Rashad, and R. Idris, "Heat transfer analysis of ethylene glycol-based Casson nanofluid around a horizontal circular cylinder with MHD effect," J. Mech. Eng. Sci., vol. 234, no. 13, pp. 2569–2580, 2020, doi: https://doi.org/10.1177/0954406220908624.

[22] H. A. Ogunseye, S. O. Salawu, and E. O. Fatunmbi, "A numerical study of MHD heat and mass transfer of a reactive Casson–Williamson nanofluid past a vertical moving cylinder," Partial Differ. Equations Appl. Math., vol. 4, p. 100148, 2021, doi: https://doi.org/10.1016/j.padiff.2021.100148.

[23] H. A. Nabwey, S. I. Alshber, A. M. Rashad, and A. E. N. Mahdy, "Influence of bioconvection and chemical reaction on Magneto—Carreau nanofluid flow through an inclined cylinder," Mathematics, vol. 10, no. 3, p. 504, 2022, doi: https://doi.org/10.3390/math10030504.

[24] T. Walelign, E. Haile, T. Kebede, and A. Walelgn, "Analytical study of heat and mass transfer in MHD flow of chemically reactive and thermally radiative Casson nanofluid over an inclined stretching cylinder," J. Phys. Commun., vol. 4, no. 12, p. 125003, 2020, doi: https://doi.org/10.1088/2399-6528/abee2e.

[25] A. S. Hamarsheh, F. A. Alwawi, H. T. Alkasasbeh, A. M. Rashad, and R. Idris, "Heat transfer improvement in MHD natural convection flow of graphite oxide/carbon nanotubes-methanol based Casson nanofluids past a horizontal circular cylinder," Processes, vol. 8, no. 11, p. 1444, 2020, doi: https://doi.org/10.3390/pr8111444.

[26] M. U. Rahman, F. Haq, M. I. Khan, F. A. Awwad, and E. A. A. Ismail, "Numerical assessment of irreversibility in radiated Sutterby nanofluid flow with activation energy and Darcy Forchheimer," Sci. Rep., vol. 13, no. 1, pp. 1–17, 2023, doi: https://doi.org/10.1038/s41598-023-46439-8.

[27] T. Walelign, E. Haile, T. Kebede, and A. Walelgn, "Analytical study of heat and mass transfer in MHD flow of chemically reactive and thermally radiative Casson nanofluid over an inclined stretching cylinder," J. Phys. Commun., vol. 5, no. 3, 2020, doi: https://doi.org/10.1088/2399-6528/abcdba.

[28] A. M. Ismaeel, R. S. Kamel, M. R. Hedar, and F. M. Hady, "Numerical simulation for a Casson nanofluid over an inclined vessel surrounded by hot tissue at the microscale," SN Appl. Sci., vol. 5, no. 8, p. 223, 2023, doi: https://doi.org/10.1007/s42452-023-05436-2.

[29] H. Yasmin, S. A. Lone, S. Anwar, S. Shahab, and A. Saeed, "Numerical calculation of thermal radiative boundary layer nanofluid flow across an extending inclined cylinder," Symmetry (Basel)., vol. 15, no. 7, p. 1424, 2023, doi: https://doi.org/10.3390/sym15071424.